A&A 439, 701–711 (2005)
DOI: 10.1051/0004-6361:20042580

Astronomy & Astrophysics

On the nature of the unidentified solar emission near 117 nm

K. Wilhelm[1], U. Schühle[1], W. Curdt[1], M. Hilchenbach[1], E. Marsch[1], P. Lemaire[2], J.-L. Bertaux[3], S. D. Jordan[4], and U. Feldman[5,6]

[1] Max-Planck-Institut für Sonnensystemforschung (MPS), 37191 Katlenburg-Lindau, Germany
e-mail: wilhelm@mps.mpg.de
[2] Institut d'Astrophysique Spatiale (IAS), Unité Mixte, CNRS-Université Paris XI, Bât. 121, 91405 Orsay, France
[3] Service d'Aéronomie du CNRS, BP 3, 91371 Verrières-le-Buisson, France
[4] NASA/Goddard Space Flight Center (GSFC), Greenbelt, MD 20771, USA
[5] Artep Inc., 2922 Excelsior Spring Ct., Ellicott City, MD 21042, USA
[6] E.O. Hulburt Center for Space Research, Naval Research Laboratory (NRL), Washington, DC 20375-5352, USA

Received 21 December 2004 / Accepted 8 April 2005

Abstract. Spectral observations of the Sun in the vacuum-ultraviolet wavelength range by SUMER on SOHO led to the discovery of unusual emission features – called humps here – at 116.70 nm and 117.05 nm on either side of the He I 58.43 nm line. This resonance line is seen in the second order of diffraction, whereas the humps are recorded in the first order with the SUMER spectrometer. In its spectra both orders are superimposed. Two less pronounced humps can be detected at 117.27 nm and near 117.85 nm. After rejecting various possibilities of an instrumental cause of the humps, they are studied in different solar regions. Most of the measurements, in particular those related to the limb-brightening characteristics, indicate that the humps are not part of the background continuum. An assembly of spectrally-unresolved atomic or ionic emission lines might be contributing to the hump at 117.05 nm, but no such lines are known near 116.7 nm. It is concluded that we detect genuine radiation, the generation of which is not understood. A two-photon emission process, parametric frequency down conversion, and molecular emissions are briefly considered as causes of the humps, but a final conclusion could not be reached.

Key words. Sun: UV radiation – atomic processes – radiation mechanisms: non-thermal

1. Introduction

Radiance spectra of the Sun in the wavelength range from 46.5 nm to 161.0 nm have been observed by the Solar Ultraviolet Measurements of Emitted Radiation (SUMER) spectrometer on the Solar and Heliospheric Observatory (SOHO) on many occasions. Some of the spectra are shown in great detail by Curdt et al. (1997, 2001, 2004). They are characterized by more than 1000 emission lines from atoms and ions, and several strong continua, specifically the recombination continua of hydrogen, oxygen, carbon, and silicon.

The multitude of emission lines makes the determination of the level of the continua difficult in some wavelength ranges of the spectrum. But, whenever the continua can be measured, the spectral radiance (away from ionization edges) is in general a monotonic function of the wavelength with marked exceptions near the He I ($1s2p\,^1P_1$–$1s^2\,^1S_0$) resonance line at 58.43 nm (seen in the second order with SUMER). We show this section of the spectrum observed in a quiet-Sun (QS) region near the centre of the Sun and in a coronal hole (CH) in Fig. 1. The symmetry of the two short-wavelength features with respect to the He I line was first noticed in the early years of the SOHO mission. Since then, many more observations of various solar regions have been performed in an effort to document the characteristics of these spectral humps (as we will call them), and to arrive at an unambiguous interpretation.

Notwithstanding these efforts, we have still not found a satisfactory explanation for these observed humps. This report summarizes the results obtained so far, and discusses the interpretations we can reject and those that might be possible. It is hoped that a unique solution will be found by involving the science community at large.

2. The SUMER instrument

The vacuum-ultraviolet (VUV) grating spectrometer SUMER has been described by Wilhelm et al. (1995a), and its performance under operational conditions has been reported by Wilhelm et al. (1997) and Lemaire et al. (1997). We list here only those aspects of the instrument that have a direct bearing on the results to be presented. Selectable slits of 0.3″, 1″ or 4″ in angular widths and 120″ or 300″ in lengths are available; alternatively a hole of 1″ diameter can be employed. The slit or hole engaged can be pointed to areas anywhere on the disk or in the low corona of the Sun. In addition, movements across the solar image in north-south and east-west directions can be executed. The smallest step size is 0.375″. A two-dimensional detector stigmatically images the slit in the spatial dimension,

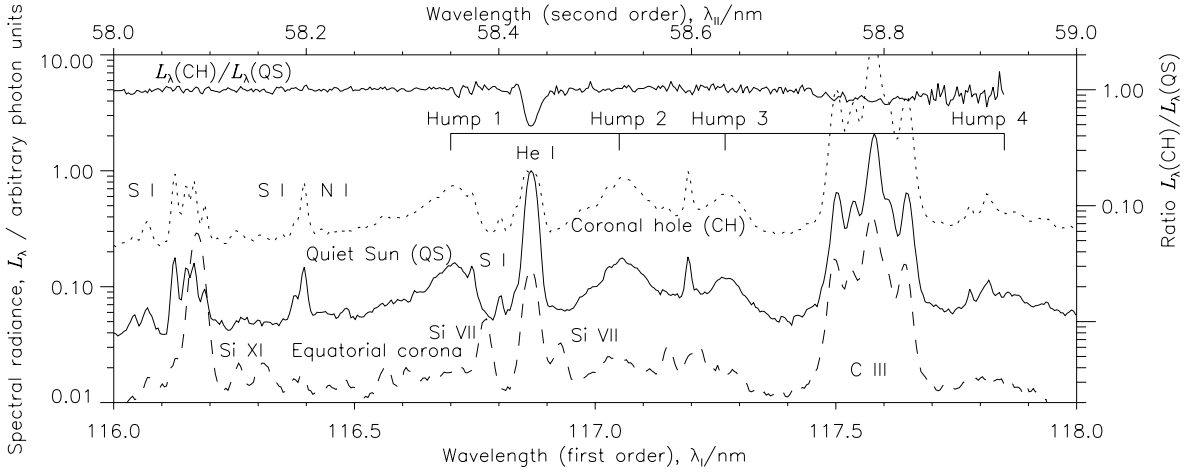

Fig. 1. Spectra of the Sun in the wavelength ranges from 116 nm to 118 nm in the first order and 58 nm to 59 nm in the second order covering the He I line at 58.43 nm and the four spectral humps. The QS spectrum observed near the centre of the Sun on 28 April 1996 is plotted as solid line, and a polar CH spectrum from 5 June 1996 as dotted line. The radiances of both spectra are normalized to the maximum of the helium line. The photon responsivity ratio is r(58 nm, KBr)/r(117 nm, KBr) = 0.12, and thus the helium line is much brighter than shown. The data of the equatorial corona ≈30″ above the west limb next to a prominence on 25 June 1996 are shown as a dashed line. A strong Si XI line can be seen at 58.08 nm in the second order, in addition to two Si VII lines in the first order at 116.77 nm and 116.93 nm. In coronal spectra of SUMER, the C III multiplet mainly consists of scattered radiation from the primary mirror. These observations were performed with detector A on the KBr photocathode. Also shown (with a scale on the right-hand side) is the spectral radiance ratio, L_λ(CH)/L_λ(QS), measured on 7 March 1999 with detector B, when sections of the slit covered both regions.

spectrally dispersed in the second dimension, covering simultaneously a wavelength interval of ≈4 nm. The instrument has two redundant detectors (A and B), which can only be used alternatively, recording overlapping, but slightly shifted wavelength ranges. The helium line is observable in both detectors in the second order of diffraction. One spatial detector pixel subtends an angle of approximately 1″, corresponding to approximately 715 km at the Sun. A spectral pixel covers 4.33 pm in the first order at 117 nm (half as much in the second order). The instrumental width with detector A is $\Delta\lambda_I$ = 5.7 pm. Under certain conditions, subpixel resolutions can be achieved in both the spatial and spectral dimensions (Wilhelm et al. 1995b).

The first and the second orders of diffraction of the concave grating are superimposed in the focal plane of the instrument. From the grating formula $m\lambda = d\,(\sin\vartheta + \sin\alpha)$, where m is the order, λ the wavelength, d the grating spacing, ϑ the angle of incidence on the grating, and α the angle of reflection, it follows that beams with λ in the first order ($m = 1$) and $\lambda/2$ in the second order ($m = 2$) are diffracted to the same detector positions as d is constant, and ϑ as well as α only change as a function of the geometry. This superposition calls for some provision to disentangle the recorded spectra. Therefore, the radiation-sensitive surfaces of the detectors are coated with a potassium-bromide (KBr) photocathode in the central sections of the dispersion direction. The remaining portions are uncoated and expose the bare microchannel plate (MCP) as cathode. The change in responsivity of the different photocathodes as a function of wavelength allows us in most cases to decide unambiguously in which order a certain radiation was detected. It is only required to shift the spectral image of the emission line or the continuum successively to both sections of the detector. The decrease in responsivity of SUMER below 50 nm (resulting from the normal-incidence optics) suppresses most of the radiation in the third and higher orders. Finally it should be mentioned that during the design and test phases of the instrument a major goal was the reduction of the internally scattered radiation. Nevertheless, this aspect has to be considered on a case-by-case basis for each critical observation.

3. Observations and data analysis

3.1. Spectral observations

As outlined in Sect. 1, unusual spectral features next to the He I line at λ_0 = 58.43344 nm (wavelength determination by Eikema et al. 1996) have been detected in SUMER spectra[1]. Their symmetry with respect to the helium line suggested a relationship, but it was – and still is – not obvious whether this symmetry is a significant feature and what exactly the generation process of the humps is. The first idea was that they might be Doppler-shifted He I radiation. Under the assumption that the humps were also observed in the second order, their peaks lie at λ_1 = 58.350 nm and λ_2 = 58.525 nm, respectively. With the help of the non-relativistic Doppler formula, we find line-of-sight (LOS) velocities of $v_1 = -410$ km s^{-1} and $v_2 = +490$ km s^{-1}, values that match the flow speed of the slow solar wind towards and (behind the Sun) away from the Earth. However, it was soon established that both humps were

[1] All raw data acquired by SUMER are in the public domain and can be obtained either from the SOHO Archive or from the SUMER Image Database at
`http://www.mps.mpg.de/english/projekte/sumer/FILE/SumerEntryPage.html`
The standard SUMER analysis and calibration software is available in the SolarSoft Library at
`http://soho.nascom.nasa.gov/solarsoft/soho/sumer`

most prominent on the disk, where the short-wavelength one should be absent if the solar wind hypothesis is correct. On the other hand, the humps are not very conspicuous in the corona as can be seen from the coronal spectrum in Fig. 1. Moreover, it was found – by placing the relevant spectral range alternatively on the KBr photocathode and the bare MCP – that the assumption made above was not correct. The humps are observed in the first order and have peak radiances at wavelengths of $\lambda_1 = 116.70$ nm (hump 1), $\lambda_2 = 117.05$ nm (hump 2), $\lambda_3 = 117.27$ nm (hump 3), and $\lambda_4 \approx 117.85$ nm (hump 4). For the full widths at half maximum we find approximately 0.095 nm for the prominent humps 1 and 2, whereas the corresponding width of the small hump 3 is about 0.070 nm. The spectral separation of the humps 1 and 2 is 0.35 nm. For humps 1 and 3 we find 0.56 nm, and ≈0.58 nm for 3 and 4. The width and the other characteristics of hump 4 cannot unambiguously be determined with the observations available.

An independent confirmation that the humps are not seen in the second order with SUMER was obtained with the Coronal Diagnostic Spectrometer (CDS) on SOHO (Harrison et al. 1995). After the first detection of the humps in the SUMER spectra, a QS region was observed by SUMER and CDS in the He I 58.43 nm line, which is recorded by CDS in the first order of diffraction. No prominent humps could be seen with CDS (A. Fludra & E. Quémerais, personal communication). This is also evident from Fig. 5 of Harrison et al. (1997) showing the He I 58.43 nm line in a QS region.

This raises the questions whether the humps 1 and 2 are related to the helium line at all (emphasized by the presence of the weaker humps 3 and 4), or – even worse – whether they are caused by some instrumental effect. One of the most likely instrumental effects could be scattered radiation from a strong solar line. It can be excluded for the helium line straightaway as the orders of diffraction are different, and any reflection inside the spectrograph would not give humps of the same shape on both detectors. Nevertheless, it is worthwhile noticing that even very strong lines, other than the C III multiplet, e.g. C III at 97.7 nm or O VI at 103.2 nm, do not show any humps. An instrumental effect related to the helium line can also be ruled out by the fact that the line-to-hump radiance ratio strongly depends on the solar region observed. The ratio of the spectral radiances in a polar CH and an adjacent QS region is $L_\lambda(\mathrm{CH})/L_\lambda(QS) \approx 1$ near 117 nm (cf. Fig. 1), but the helium line shows, of course, the well-known CH darkening. Relative to the peak spectral radiance of the He I line, the humps are thus much more pronounced in CH than in QS regions.

Taken all findings together, we can discard an artifact caused by the helium line. Yet these arguments do not repudiate an influence of the continuum radiation. A very subtle effect would be the Wood grating anomaly. It can cause variations of the diffraction efficiency as a function of wavelength for a grating illuminated by continuum radiation (Wood 1902). The explanation for this effect was given by Rayleigh (1907). It is based on the idea that a high diffraction order of the beam propagates along the surface of the grating for certain angles of incidence before it is diffracted off to the detector. Using the detailed theory presented by Palmer et al. (1975), we checked the SUMER optical design for potential spectral ranges where the Wood anomaly might have an effect, and found 55.3 nm and 69.5 nm in the second order as well as 92.0 nm and 138.5 nm in the first order, not anywhere near the spectral positions of the humps. Even at the suspected ranges, we could not detect any unusual features, and conclude that SUMER is not susceptible to the effects of the Wood anomaly; in all likelihood, because of the concave grating employed, whereas the Rayleigh theory requires a plane grating.

Detector anomalies in the spectral or spatial dimensions can be excluded by the assertion that the humps have been observed at many different pixel positions. Unless there is a systematic effect that escaped detection until now, it also cannot be a detector problem, because the humps have been recorded with both SUMER detectors. Another possibility could be that the wavelength responsivity of SUMER, defined during the radiometric calibration process, introduces the observed continuum variations. However, there is no change of the response function on the scale of 1 nm or less at 117 nm on either the bare MCP or the KBr photocathode (cf. Wilhelm et al. 2002). If, on the other hand, such a variation was actually present and had not been recorded during the calibration procedure with distinct spectral lines, the strange fact would remain that both photocathodes with independent spectral calibrations show the humps.

Limb observations with the Skylab S082B slit spectrograph (Bartoe et al. 1977), as reported by Feldman & Doschek (1991), also show the humps 1 to 4. This wavelength range is recorded in the second order by S082B. Higher orders cannot be superimposed, because the Al + MgF_2 optical coatings limit the responsivity at shorter wavelengths, and thus the He I 58.43 nm line is not seen. The fact that the humps are observed by two completely independent and quite different instruments is another very strong argument that they are of solar origin and not any instrumental artifacts. The humps can even be seen in spectra of the spectroscopic binary system Capella (G8 III + G1 III) obtained by the Far Ultraviolet Spectroscopic Explorer (FUSE) presented by Young et al. (2001). We also found them in observations of α Cen A (G2 V) published by Redfield et al. (2002), whereas the presence of the humps in Procyon and some other late-type dwarf stars is uncertain.

We are thus led to the conclusion that we detect actual humps of radiation, and have to ask ourselves whether they may consist of a large number of unresolved atomic emission lines or whether the continuum has, for unknown reasons, this particular shape. To answer these questions, observations are required that might allow us to distinguish between the humps, lines emitted by neutrals or other particles, and the normal continuum of the solar chromosphere.

3.2. Spatial and temporal variations of the chromospheric network

A raster scan in a QS region covering the wavelength range shown in Fig. 2 has been inspected for any clues as far as the spatial variations are concerned. The humps could not be integrated over their full wavelength extension, because some obvious emission lines had to be excluded. The selected ranges thus take only a fraction of the hump radiation into account.

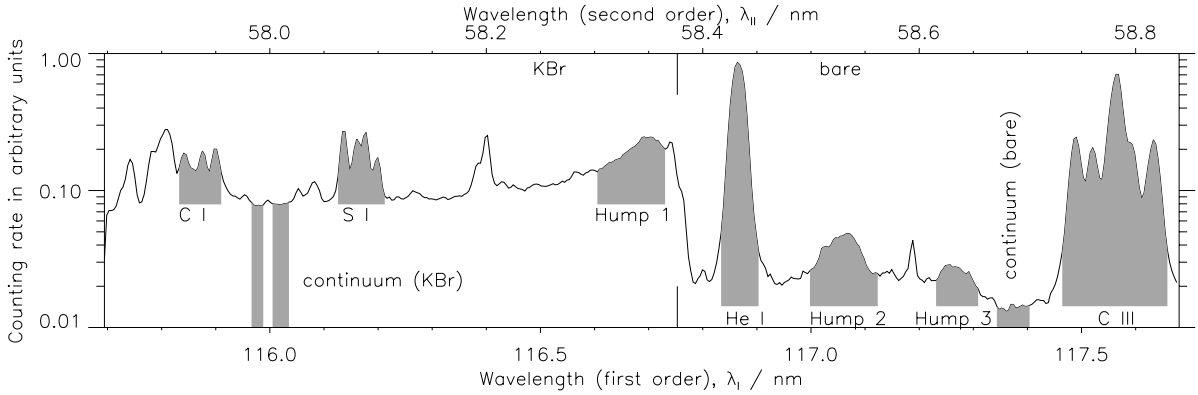

Fig. 2. Spectral range of the raster scan shown in Fig. 3. The sections of the spectrum used for compiling the maps are indicated. The observations were performed with detector B and the 1″ × 300″ slit. Note that the short-wavelength hump 1 was put on the KBr photocathode, whereas the long-wavelength humps 2 and 3 were on the bare MCP in this case.

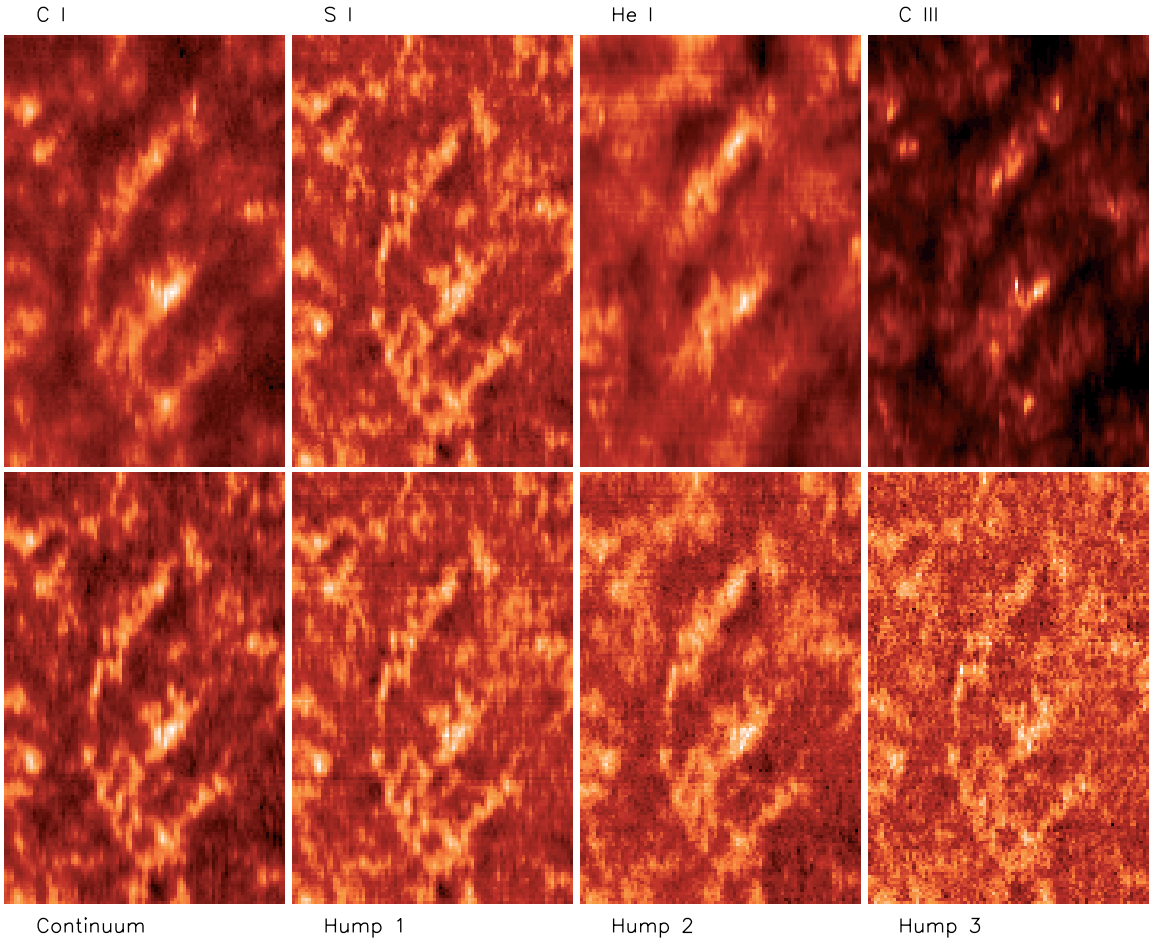

Fig. 3. A QS area simultaneously recorded during a single raster scan in various VUV emissions. *Upper row*: C I and S I (on KBr); He I and C III (on the bare MCP). *Lower row*: continuum; hump 1 (KBr); humps 2 and 3 (bare). The continuum is subtracted as background from the other emissions. The area has a N–S extension of 110 Mm and an E–W extension of 71 Mm. The observations were made near the centre of the Sun on 26 February 1999.

The fraction is approximately two thirds and is the same in all applications here. The maps simultaneously produced in various emission lines, the humps, and the continuum are shown in Fig. 3. They indicate that the humps 1 to 3 give maps of the chromospheric network structure that are virtually identical (considering the lower counting rates for the humps 2 and 3 on the bare detector), but differ strikingly from the He I and C III maps, and somewhat from the C I map. The S I map, however, is so similar to those of the humps that a distinction is not possible in this way, and the situation of the continuum is unclear. The structures emitting the humps appear to be sharper than those of the He I line.

Table 1. Linear correlation coefficients, r, between the chromospheric network maps shown in Fig. 3. *Upper part*: with respect to hump 1; *lower part*: with respect to C III lines. Values for the total areas are given as well as for the lane and cell regions.

r	Hump 2	Hump 3	Continuum	C I lines	S I lines	He I line	C III lines
Hump 1							
Total	0.835	0.783	0.886	0.732	0.941	0.464	0.485
Lane	0.767	0.706	0.830	0.642	0.904	0.355	0.408
Cell	0.439	0.451	0.497	0.138	0.754	0.010	–0.042
C III lines							
Total				0.819	0.530	0.635	
Lane				0.812	0.459	0.603	
Cell				0.719	0.100	0.544	

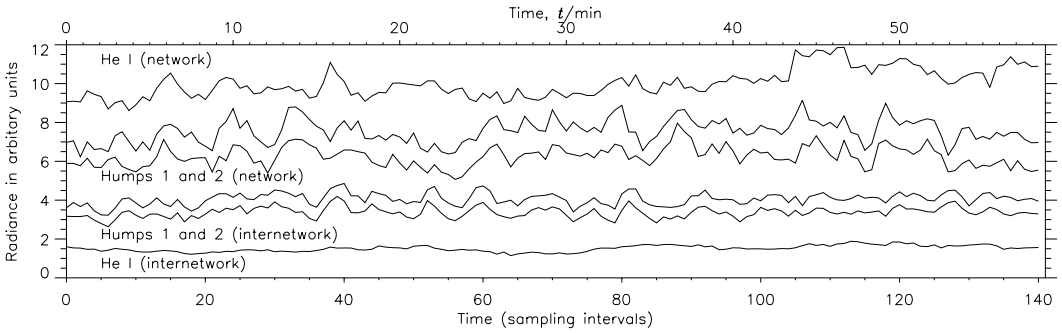

Fig. 4. Temporal variations of the radiances of the helium line and the humps 1 and 2 in a QS region separated into network and internetwork areas. The exposures were taken with detector A and the 1″ × 120″ slit. A bright section of 16″ in the helium line was considered to represent a network lane, and an adjacent darker section of 19″ an internetwork region.

These visual impressions are confirmed by the results in Table 1, where linear correlation coefficients between the hump 1 and the other emissions are compiled. We have also calculated the correlation between some of the emission line pairs, and have split the maps into network lanes and internetwork (cell) areas of equal sizes on the basis of the S I data. The correlation between lane regions is greater than between cell areas in all cases. In the internetwork, He I and C III are not at all related to hump 1. On the other hand, there is a strong correlation of hump 1 with S I in all regions, in contrast to the C I line, which is, however, closely related to C III. The poor counting statistics for the humps 2 and 3 on the bare MCP must be taken into account, when considering the relatively low values of the hump pairs in cell areas. From these results, we conclude that the humps are emitted from levels very deep in the solar atmosphere, much cooler than those that emit the He I and C III lines.

The temporal variations were investigated with detector A on 17 November 2004. The humps 1 and 2 and the helium line were observed with a cadence of 25 s in a QS region for 1 h. Along the slit, bright and dark sections have been identified as network lane crossings and internetwork areas. The variations of two adjacent sections are shown in Fig. 4. A very close relationship can be seen between humps 1 and 2 in the network lane and, in particular, in the internetwork with correlation coefficients of $r_N = 0.822$ and $r_I = 0.896$, respectively. The relationship between the humps and the helium line is much weaker with $r_N = 0.272$ and $r_I = 0.180$ as could be expected from the corresponding spatial results. The hump variations in the adjacent network and internetwork regions are unrelated ($r_{N,I} = 0.044$).

3.3. Limb observations

In an attempt to measure the height above the limb of the source regions of the various emissions with the best spatial resolution the SUMER instrument can furnish, the limb brightening curves of the humps, the continuum, and the emission lines near 58.43 nm were determined with detector B and subpixel precision in a polar CH on 2 May 2004. The 0.3″ × 120″ slit crossed the limb in north-south direction near the south pole. The telescope pointing was then moved outwards along the slit in steps of 0.375″ between exposures. During the first 32 steps the helium line and its environment were recorded on KBr, while it was placed on the bare MCP in a later sequence.

Since eight steps shift the image on the detector by 8 × 0.375″ = 3″ or three spatial pixels, subpixel integration can be achieved by digitally expanding the spatial dimension of the data array by a factor of eight, i.e. 0.125″ (or 90 km) per subpixel, and adding the arrays after repeated shifts of three subpixels. The result is shown in Fig. 5 as high-resolution limb spectrum with humps 1 to 3 on KBr. About 68″ of the slit length are displayed. The humps exhibit a slight structuring along the dispersion direction with a peak-to-peak separation of ≈24 pm. It is unclear what causes this structure, in particular in the hump 1 as there are no cool emission lines known in this wavelength range. However, it is very likely that the MCP microstructure is responsible for the effect, since we only have a

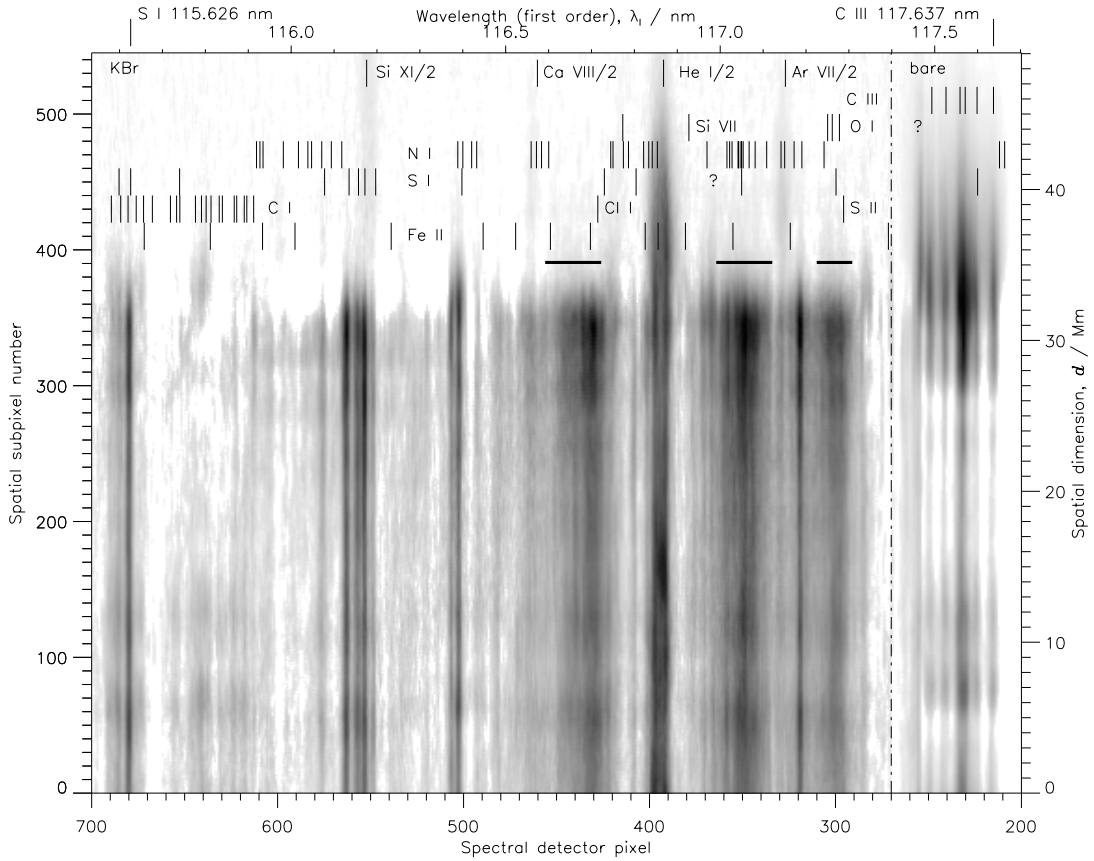

Fig. 5. Stigmatic limb spectrum with humps 1 to 3 on the KBr photocathode of detector B. The C III multiplet was recorded on the bare MCP. The spectral ranges selected for further analysis of the humps are indicated by horizontal bars. The continuum background was subtracted. The spectral calibration was obtained from the S I line at 115.627 nm and the C III line at 117.637 nm (both shown in the upper margin). The spectral positions of the known C I, S I, N I, Cl I, S II, Fe II, and C III lines in this range are marked by vertical bars. The lines seen in the second order and the Si VII lines are taken from Feldman et al. (1997). Two lines could not be identified.

five-year-old flatfield available for the image correction of the 2004 data. This view is supported by the observation that the spectra in Figs. 1 and 2 with much better flatfield corrections do not show such a structure. The C I, N I, O I, S I, Cl I, S II, and Fe II lines in this wavelength range given by Kelly (1987) and Martin et al. (2005)[2] are shown on top of the spectrum. Only calculated wavelengths are known for the three O I lines. If we were indeed observing them, they would, however, be resolved in our spectrum (cf. N I and S I lines near 116.4 nm). Judged from these data that include all known wavelengths of abundant atoms and singly-charged ions in this range, only hump 2 might have significant contributions from an assembly of N I lines.

The limb scans are displayed in Figs. 6a and 7a for both sequences as individual limb brightening curves, and in Figs. 6b and 7b as ratios of the hump radiance relative to other emissions. The helium line is blended by first-order contributions of N I lines. The amount of the contributions is different on the KBr photocathode or the bare MCP. In principle, these blends have to be taken into account when the hump-to-line ratio is calculated, but it has been shown that the relative contributions in a window of 0.11 nm around the line are only 4% on KBr and 1% on the bare MCP (Wilhelm et al. 1998), and can be neglected in our narrower interval. Relative to the N I and S I lines, the C I lines are much weaker near the limb (cf. Fig. 5) and, therefore, have not been considered in Fig. 6. Whereas the N I and S I lines in this wavelength range exhibit a limb brightening, C I is even darkened there. This is not related to the CH conditions as the C I lines are rather prominent in equatorial CHs (cf. Curdt et al. 2001). The depletion of carbon in the outer layers of the chromosphere could indicate the formation of CO in very cool plasma regions (Ayres & Rabin 1996), although there are still many open questions concerning the thermal structure of the upper chromosphere.

We have calculated the hump-to-helium ratio under the assumption that the humps are observed in the first or second order, and all radiances have been measured in photon units. The good agreement evident for the KBr photocathode and the bare MCP in the first case, deteriorates in the second case by more than a factor of three (cf. Figs. 6b and 7b), which results from the responsivity ratio of SUMER: $R_{117}/R_{58} = 3.53$, where $R_{117} = r(117\,\mathrm{nm}, \mathrm{KBr})/r(117\,\mathrm{nm}, \mathrm{bare}) = 7.03$ and $R_{58} = r(58\,\mathrm{nm}, \mathrm{KBr})/r(58\,\mathrm{nm}, \mathrm{bare}) = 1.99$ (Wilhelm et al. 2002). This confirms that the humps 1 and 2 are seen in the first order at wavelengths approximately twice that of the He I line. From the response of the humps 3 and 4 on both photocathodes, it is clear that they are recorded in the first order, too.

[2] Available from `http://physics.nist.gov/PhysRefData/ASD/lines_form.html`.

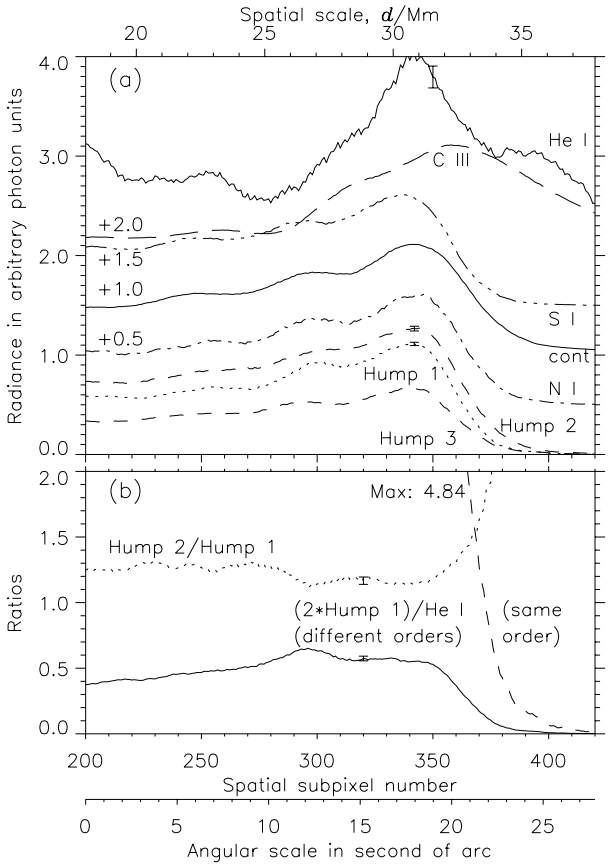

Fig. 6. a) Limb brightening curves of spectral features displayed in Fig. 5. The radiances of the He I line and the humps 1 to 3 are given in arbitrary (photon) units (the same for all four of them). The spectral radiances of the continuum and the other emission lines are normalized to the hump 1 (not blended by N I contributions) and displaced in steps of 0.5 to avoid confusion. Based on the counting statistics, some standard uncertainties are indicated. The N I line is that at 117.195 nm, where Kelly (1987) lists a N I line, albeit with much lower relative radiance than observed. The identification therefore is tentative. **b)** Ratios of the hump 2/hump 1 radiances and of twice the first-order hump 1 relative to the helium line. The latter ratio is also shown as dashed line under the assumption that the hump is seen in the second order with a maximum off the scale.

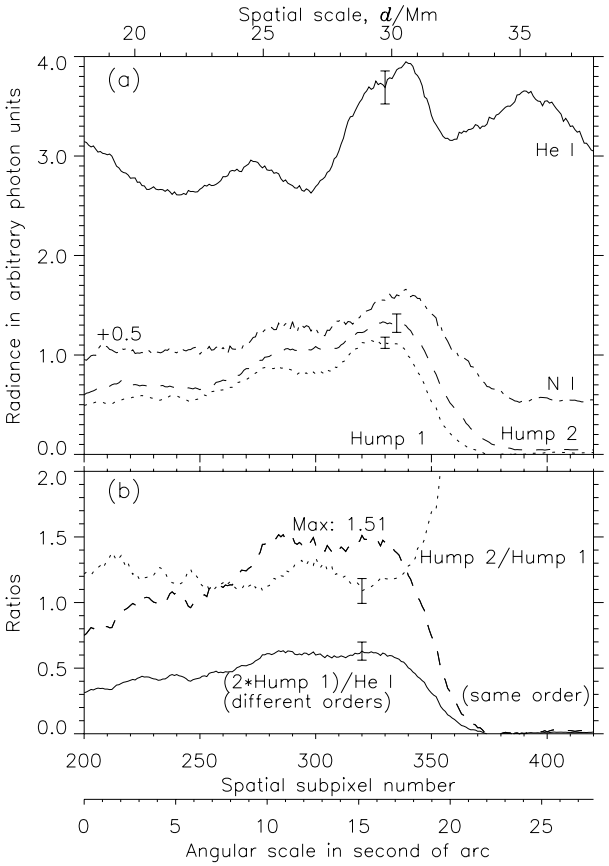

Fig. 7. Limb observations on the bare MCP with adequate counting statistics. The lower rates lead to somewhat larger standard uncertainties than for KBr. The radiance ratio of hump 1 to helium is virtually identical to that of the KBr case if different orders are assumed, but is very different for the same order (dashed line) (cf. Fig. 6b).

The diagrams in Figs. 6a and 7a support the distinction between the He I line and the other emissions presented in the raster scan in Sect. 3.2, but also provide some evidence that the humps and the S I, N I and C III lines behave differently. According to the data displayed in Fig. 5, some N I blends and one S I line contribute to the hump 2, and could cause its higher radiance relative to the hump 1. Only isolated chromospheric lines (with respect to the SUMER resolution) are known to contribute to the humps 2 and 3, and, therefore, it is unlikely that they consist of an assembly of unresolved emission lines. The increase of the radiance ratio above the limb might be related to the effect of the N I blends in hump 2. The limb brightening curves of the continuum and the humps are rather similar, but a slight shift of the continuum curve towards greater heights is present in Fig. 6a. Because of the broad maxima of the limb-brightening curves, the positions of the peak radiances cannot directly be determined with subpixel accuracy. To arrive at quantitative results, a cross-correlation analysis was performed. It was carried out over the range of the strong limb brightening (subpixels 270 to 390). The results are given in the first row of Table 2. We find a shift of the continuum of about 540 km to greater heights with respect to the hump 1.

At this juncture, a word of caution might be in order as to the meaning of the emission heights obtained. The solar chromosphere is clearly not only structured in height, but also in both horizontal dimensions as indicated by the network lanes in Fig. 3. It is, in addition, very dynamic and is varying on many temporal scales. Our limb-brightening curves integrated along the LOS and over about 1 h in time can thus only provide average values of the emission heights. We see this as an advantage, though, as it would be virtually impossible to untangle individual events, even if the spatial and temporal resolutions of the instrument would be adequate for such a task.

The low formation height of the S I line relative to the N I line and the humps is surprising. However, it has to be noted that the spatial positions of the limb brightening curves of certain emissions could, in principle, be a function of the wavelength, if the detector correction procedure left a residual inclination of the spectrum with respect to the pixel matrix. Such an effect is likely to increase with the spectral separation of the emissions under study, and thus the S I lines near

Table 2. Height differences, Δh, of solar emission with respect to the hump 1 obtained by cross-correlations calculations between limb brightening curves from slit (Fig. 6a) and hole (Fig. 8) observations. The rows named "average" refer to averages above the horizontal dashed-dotted lines.

Δh/km	Fig. 6a	Fig. 8a (N)		Fig. 8b (S-W)	
		peak	average	peak	average
Hump 2	90	0	80	0	40
Hump 3	–50	0	–210	0	–60
Continuum	540	540	470	270	320
N I	270	0	120	180	130
S I	–180	0	160	0	100
C III	3300				

116.2 nm would be affected most. We have, therefore, checked the position of the lower slit end on the detector and found it well aligned with the dispersion direction in the final data product obtained with the SUMER analysis software. Since we are working with spatial subpixel resolution, and in order to eliminate with certainty any detector effect in this context, further limb scans were made on 1 and 2 December 2004 with the 1″ hole in the SUMER slit plate. The radiation from the hole is uniquely related to its spatial position with respect to the solar disk image, even if it is diffracted on different spatial detector pixels as a function of wavelength. A limb scan with the hole was performed with detector A near the north pole, and another one in the south-west at a heliographic latitude of ≈−20° with spatial step widths of 0.375″ in the north-south direction. One step only changes about one third of the field of view defined by the 1″ hole, and corresponds to ≈270 km in Fig. 8a, whereas in Fig. 8b the geometry leads to a change in height of ≈90 km per step. The cross-correlation curves in Fig. 8 are not symmetric. Therefore, the shifts given in the last four columns of Table 2 are found both from peak correlation values and weighted averages of the correlation functions. An assessment of the actual spatial resolution is difficult. The shift between the humps 1 and 2 was less than 100 km in all cases. Thus we adopt the attitude that we have to look for a shift of at least twice as much before it can be considered to be significant.

C III again lies above 3000 km, and is not included in these calculations. It is immediately clear that the S I lines originate in a region much closer to the N I line than suggested in the first column of Table 2. The detector correction algorithm is obviously not perfect enough to compare lines with rather large wavelength differences on a spatial subpixel scale. However, for the humps and the continuum we find very similar shifts with both detectors in the May and December 2004 observations yielding a mean difference between the humps and the continuum of 430 km.

3.4. Prominence and filament observations

Prominences are conspicuous features when seen in the He II 30.38 nm line (cf. Moses et al. 1997) as well as in the He I 58.43 nm line discussed here. We have observed

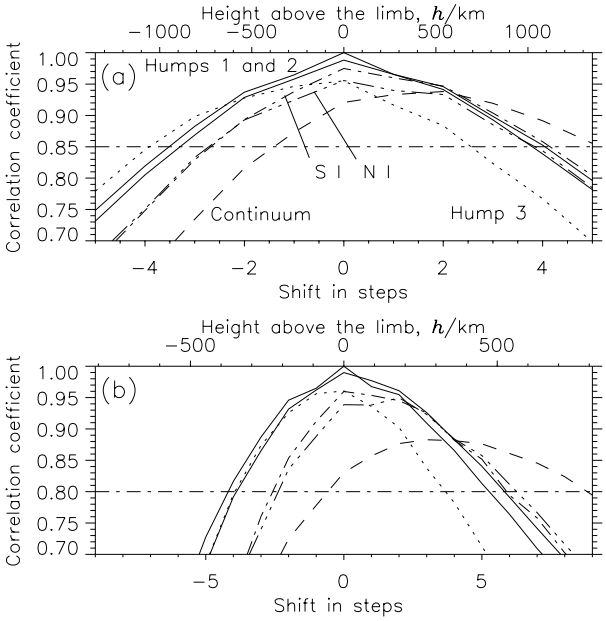

Fig. 8. Cross-correlation analyses of the limb scans with the 1″ hole, plotted with respect to the peak position of hump 1. **a)** North pole: one step corresponds to ≈270 km in height (upper scale). Details on the relative shifts are compiled in Table 2. **b)** South-west limb: here one step corresponds to ≈90 km in height. The shifts are in reasonable agreement with those in panel **a)** and are also given in Table 2.

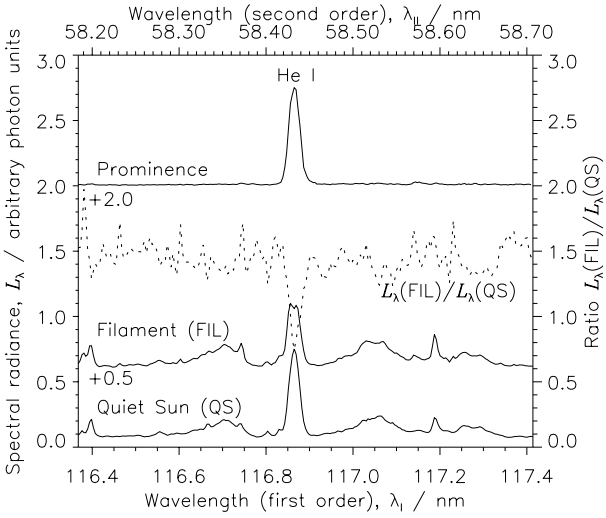

Fig. 9. Prominence and filament observations in May 2004 in comparison with a QS area. The filament radiance is displayed 0.5 higher than the QS scale; the prominence spectrum is shifted by 2.0. The peak spectral radiance of the helium line in the prominence is normalized to the corresponding QS value. Also shown is the ratio of the spectral radiances L_λ(FIL)/L_λ(QS).

the humps 1 to 3 and the helium line in a prominence on 7 May 2004. Figure 9 shows that the humps are almost absent in the prominence spectrum. Similarly, we have studied the situation in a filament on 27 May 2004 and compared it with a QS region close by. The relative increase of the spectral radiance of the humps and the adjacent emissions over the filament is ≈50% with respect to the QS level, whereas the

He I spectral radiance at line centre is smaller by 25% (dotted line in Fig. 9). These observations again indicate that the radiation of the humps is not directly related to that of the helium line, but do not exclude a coupling of the generation processes modified, for example, by the different optical depths of the solar atmosphere and its structures for the hump and helium wavelengths.

The He I line is self-reversed over the filament and in some areas of the polar CH, in particular, near the limb, but not everywhere (see Fig. 5 near spatial subpixels 340 and 180). Neither in a prominence nor in QS regions an inversion was found, confirming the QS results of Doschek et al. (1974). The QS profiles are difficult to reconcile with those calculated by Fontenla et al. (2002).

3.5. Sunspot observations

In sunspot spectra, shown by Curdt et al. (2001), the He I spectral radiance is a factor of approximately four larger than in QS regions, and the humps are fainter by ≈2. In a SUMER reference spectrum of 17 December 1996, this line is enhanced over a sunspot relative to the surrounding active plage (and the neighbouring QS), whereas the humps are lower than in the plage region (and the QS). Weaker hump emission over a sunspot was also observed by Schühle et al. (1999).

4. Interpretation

It has been shown that the humps observed by SUMER can neither be explained as an instrumental artifact nor is it likely that the humps, in particular humps 1 and 3, are an assembly of unresolved emission lines with low formation temperatures. Their limb brightening was significantly different from the behaviour of the continuum radiation, and thus it is very unlikely that they are part of the normal continuum. So, what are they? The symmetry of two of the humps with respect to the He I 58.43 nm line might suggest a relationship, however, it cannot be excluded that the humps are entirely unrelated to it. Even in this case, the unusual spectral shape of the humps calls for an explanation.

The generation processes of the helium lines He II at 30.38 nm and He I at 58.43 nm in the solar atmosphere are still a matter of debate (Jordan 1975; Andretta & Jones 1997; Macpherson & Jordan 1999; Andretta et al. 2003; Ravindra & Venkatakrishnan 2003; Judge & Pietarila 2004). It is, however, undisputed that the upper chromosphere is optically dense for the He I 58.43 nm line (Avrett 1999). The optical depth of this line is $\tau_{58.4} = 10\,000$ at line centre (cf. Gallagher et al. 1998). Depending on where in the atmosphere the 58.43 nm emission is produced, up to 1000 absorption and re-emission events can occur before a photon can escape. At wavelengths near 117 nm, however, the plasma of the upper chromosphere is optically thin (cf. the raster maps in Fig. 3 and the limb brightenings of the continuum and in the humps in Figs. 6a and 7a) and any such photon generated there would be radiated away, or lost in the lower chromosphere. Thus, if we could conceive processes that either would produce two photons in the He I $1s2p\,^1P_1$–$1s^2\,^1S_0$ transition or, alternatively, could split a single photon emitted by the helium atom into two, the solar upper chromosphere would provide a strong amplification for the low-energy photons with respect to the 58.43 nm radiation. There are, in fact, such processes, namely "two-photon emission" and "parametric frequency down conversion", and we have to explore whether one of them, or both, might be pertinent here. We also have to consider whether emissions from species other than helium could be involved.

4.1. Two-photon emission

The general principle of the two-photon emission was originally discussed by Göppert-Mayer (1931). It was further studied by many authors (Breit & Teller 1940; Spitzer & Greenstein 1951; Shapiro & Breit 1959; Drake & Dalgarno 1968; Bely & Faucher 1969). The simultaneous emission of the photons requires two electric dipole transitions to and from a virtual intermediate state (e.g. S–P, P–S transitions in hydrogen-like systems or $2\,^1S_0$–$n\,^1P_1$, $n\,^1P_1$–$1\,^1S_0$ in helium-like ones), or two corresponding transitions, but with a mixing process in between: $2\,^3S_1$–$n\,^3P_1 \rightarrow n\,^1P_1$–$1\,^1S_0$. To answer the question whether two-photon transitions from the helium $2p\,^1P_1$ state could be the cause of the spectral observations of SUMER near 58.43 nm and 2×58.43 nm, the first step would be to demonstrate this possibility in principle. The next step would then be a quantitative evaluation including the radiation transfer considerations.

As far as the first step is concerned, we know of no previous treatments involving a resonance line. Göppert-Mayer (1931) concluded that the two-photon emission could only be observed in transitions from metastable states, because of the short lifetimes of energy levels depopulated by allowed transitions – Johansson et al. (2003) found in helium that $\tau(1s2p\,^1P_1) = 0.57\,ns$ – and the inherent low probability of a two-photon decay. This, however, does not preclude an observation from allowed transitions under special circumstances.

In evaluating the probability of the simultaneous emission of two photons, the sum over intermediate states has to be extended into the continuum (Breit & Teller 1940; Mathis 1957; Drake & Dalgarno 1969). The conservation of energy is not required for the intermediate state, but must, of course, be satisfied for the complete process. The question now is, whether electric-dipole transitions from $2\,^1P_1$ to the continuum and from there to $1\,^1S_0$ would give a finite two-photon emission probability. As far as we can see there are no other routes available in helium.

Mixing of $2p\,^1P_1$ and $2s\,^3S_1$ with a probability of $\leq 10^{-5}$ (Breit & Teller 1940) followed by a two-photon emission from $2s\,^3S_1$ should occur; it would, however, give a central wavelength of 2×62.71 nm, corresponding to the $2\,^3S_1$–$1\,^1S_0$ transition. The spectral range near 125 nm is crowded with many emission lines making a determination of the continuum level impossible, and any such two-photon emission, even if it were there, could not be identified. Similarly, there should be a two-photon emission from the $2\,^1S_0$ state at a central wavelength of 2×60.14 nm, but unless this radiation is very pronounced it would be hidden in the blue wing of H I Lyα.

Another important question is the spectral distribution of the two photons one can expect. A symmetric distribution with a maximum at half the total transition energy is found for He I $2\,^1S_0$–$1\,^1S_0$ (Dalgarno 1966), but a minimum occurs at the centre with two humps on either side for the He I $2\,^3S_1$–$1\,^1S_0$ transition (Drake & Dalgarno 1968; Bely & Faucher 1969). This is a consequence of the total angular momentum to be transported by the photons and their Bose-Einstein statistics (Mokler & Dunford 2004). Our case would be equivalent to the $2\,^3S_1$–$1\,^1S_0$ situation, but it has to be noted that the theoretical distributions calculated for the intercombination line are much wider than those observed in our case. Whether an allowed transition or special conditions in the solar atmosphere would give such a modified distribution has yet to be determined.

There are a few reports on observational confirmations of two-photon emissions from metastable states in hydrogen and helium-like ions. We mention here that Elton et al. (1968) observed a prominent peak in the continuum near 3.2 nm emitted from a hot plasma with neon impurities. The radiation is associated with the second-order two-photon decay of the $2\,^1S$ state of helium-like Ne IX. A two-photon continuum of the metastable 2 S state of hydrogen has been seen with the International Ultraviolet Explorer (IUE) in the spectrum of Herbig-Haro Object 2H (Brugel et al. 1982). The spectral distributions are consistent with the theoretical results; in fact, they are the main reason for the identification of the two-photon continua.

4.2. Parametric down conversion

The parametric production of photon pairs was first observed by Burnham & Weinberg (1970). A quantum mechanical description has been given by Mollow (1973). A theory of the parametric frequency down conversion – the spontaneous splitting of a photon into lower frequency "signal" and "idler" photons – has been formulated by Hong & Mandel (1985). Recent studies of the Spontaneous Parametric Down Conversion (SPDC) concentrate on sources of entangled photon pairs in the conversion process (cf. Kwiat et al. 1995; Banaszek et al. 2001) or their correlation properties (Rubin 1996). The energy and momentum of the involved photons are conserved. The photon splitting is achieved in the laboratory via non-linear optical crystals, the refractive index being a function of the wavelength and propagation direction. While the two-photon process described in the previous paragraphs are likely to give a broad emission spectrum, the conservation of the momentum in the down conversion process should result in two narrow emissions, but no quantitative statement can be made at this stage.

We can only think of the magnetic field that might introduce such a double refractive index in the solar atmosphere via the Voigt effect (cf. Budker et al. 2002). The known field strengths are, however, far too weak to explain the observed line shift, and thus this effect is probably not of any importance here.

4.3. Molecular emissions

The spectral shape might indicate that the humps are due to molecular fluorescence excited by either the He I line or another strong emission line. Strong fluorescence of molecular hydrogen excited by the H I Lyα and the O VI 103.2 nm lines is well known since its first observation with the High Resolution Telescope and Spectrograph (HRTS) (Jordan et al. 1977). The emission of neutral molecular hydrogen is most prominent in sunspots and much less in QS areas. However, the hump emission reported here is weak over a sunspot. This makes it unlikely that we observe fluorescence of neutral molecular hydrogen. The excitation of molecular hydrogen by the He I 58.43 nm line, on the other hand, would be well above the ionization limit, and could be enhanced by coincidence with autoionizing Rydberg states. However, such an excitation path is not known to us.

Excitations of molecular hydrogen ions and other, possibly abundant, species, such as carbon monoxide (CO), free hydroxyl (OH), or carbohydrate (CH), have to be investigated further, and the emission of excimer molecules, e.g. HeH, must be considered as well. Near-ultraviolet fluorescence of excited states of HeH (HeH^*) has first been observed by Möller et al. (1985) after excitation with synchrotron radiation in the VUV range. Predissociation and radiative dissociation of HeH^* have been reported by Peterson & Bae (1986). In both cases, the radiative decay was observed as continuum emission below 10 eV. VUV fluorescence of HeH was observed between 140 nm and 160 nm by Tokaryk et al. (1989). The radiation was emitted in a broad band due to the repulsive limb of the ground state. Highly excited states of this excimer molecule that can possibly be populated by strong solar lines above 10.6 eV are well known. To our knowledge this emission has, however, not been detected at the wavelengths considered in this report.

5. Conclusion

We have shown that the conspicuous humps in the SUMER spectra on either side of the He I 58.43 nm line (seen in the second order) are caused by VUV radiation near 116.70 nm and 117.05 nm (in the first order). Although the total radiance in the hump 2, which contains some blends, was consistently larger than that of hump 1, all other characteristics were found to be the same, but most of them distinct from those either of the background continuum or emission lines. Two-photon emission, parametric down conversion in frequency, and molecular emissions have been considered as causes of the spectral features, but a final conclusion could not be reached.

Our attention has been focussed on the prominent humps 1 and 2 near the helium line, where they were first detected. However, there are smaller such features near the C III multiplet, called humps 3 and 4. They are observed in the same order as C III. Should they be linked to the multiplet, a two-photon concept could be ruled out here. Alternatively, one could ask whether these smaller features, in particular hump 3, are in some way related to the humps 1 and 2, because this hump displays characteristics similar to those of humps 1 and 2, except

for a somewhat narrower spectral width. So finally, we have to conclude that many questions remain unanswered in explaining the SUMER observations of the spectral humps, which are presented here to stimulate a discussion in the science community.

Acknowledgements. The SUMER instrument and its operation are financed by the Deutsches Zentrum für Luft- und Raumfahrt (DLR), the Centre National d'Études Spatiales (CNES), the National Aeronautics and Space Administration (NASA), and the European Space Agency's (ESA) PRODEX programme (Swiss contribution). The instrument is part of ESA's and NASA's Solar and Heliospheric Observatory (SOHO). We thank Bernhard Fleck for his encouragement to pursue this study, and the referee, Vincenzo Andretta, for his very constructive criticism of the manuscript.

References

Andretta, V., & Jones, H. P. 1997, ApJ, 489, 375
Andretta, V., Del Zanna, G., & Jordan, S. D. 2003, A&A, 400, 737
Avrett, E. H. 1999, in Proc. 8th SOHO Workshop, Plasma Dynamics and Diagnostics in the Solar Transition Region and Corona, ed. J.-C. Vial, & B. Kaldeich-Schürmann, ESA SP-446, 141
Ayres, T. R., & Rabin, D. 1996, ApJ, 460, 1042
Banaszek, K., U'Ren, A. B., & Walmsley, I. A. 2001, Opt. Lett., 26, 1367
Bartoe, J.-D. F., Brueckner, G. E., Purcell, J. D., & Tousey, R. 1977, Appl. Opt., 16, 879
Bely, O., & Faucher, P. 1969, A&A, 1, 37
Breit, G., & Teller, E. 1940, ApJ, 91, 215
Brugel, E. W., Shull, J. M., & Seab, C. G. 1982, ApJ, 262, L35
Budker, D., Gawlik, W., Kimball, D. F., et al. 2002, Rev. Mod. Phys., 74, 1153
Burnham, D. C., & Weinberg, D. L. 1970, Phys. Rev. Lett., 25, 84
Curdt, W., Feldman, U., Laming, J. M., et al. 1997, A&AS, 126, 281
Curdt, W., Brekke, P., Feldman, U., et al. 2001, A&A, 375, 591
Curdt, W., Landi. E., Feldman, U., et al. 2004, A&A, 424, 1045
Dalgarno, A. 1966, MNRAS, 131, 311
Doschek, G. A., Behring, W. E., & Feldman, U. 1974, ApJ, 190, L141
Drake, G. W. F., & Dalgarno, A. 1968, ApJ, 152, L121
Drake, G. W. F., & Dalgarno, A. 1969, ApJ, 157, 459
Eikema, K. S. E., Ubachs, W., Vassen, W., & Hogervorst, W. 1996, Phys. Rev. Lett., 76, 1216
Elton, R. C., Palumbo, L. J., & Griem, H. R. 1968, Phys. Rev. Lett., 20, 783
Feldman, U., & Doschek, G. A. 1991, ApJS, 75, 925
Feldman, U., Behring, W. E., Curdt, W., et al. 1997, ApJS, 113, 195
Fontenla, J. M., Avrett, E. H., & Loeser, R. 2002, ApJ, 572, 636
Gallagher, P. T., Phillips, K. J. H., Harra-Murnion, L. K., & Keenan, F. P. 1998, A&A, 335, 733
Göppert-Mayer, M. 1931, Ann. Phys., 9, 273
Harrison, R. A., Sawyer, E. C., Carter, M. K., et al. 1995, Sol. Phys., 162, 233
Harrison, R. A., Fludra, A., Pike, C. D., et al. 1997, Sol. Phys., 170, 123
Hong, C. K., & Mandel, L. 1985, Phys. Rev. A, 31, 2409
Johansson, A., Raarup, M. K., Li, Z. S., et al. 2003, Eur. Phys. J. D, 22, 3
Jordan, C. 1975, MNRAS, 170, 429
Jordan, C., Brueckner, G. E., Bartoe, J.-D. F., et al. 1977, Nature, 270, 326
Judge, P. G., & Pietarila, A. 2004, ApJ, 606, 1258
Kelly, R. L. 1987, J. Phys. Chem. Ref. Data, 16, 1
Kwiat, P. G., Mattle, K., Weinfurter, H., et al. 1995, Phys. Rev. Lett., 75, 4337
Lemaire, P., Wilhelm, K., Curdt, W., et al. 1997, Sol. Phys., 170, 105
Macpherson, K. P., & Jordan, C. 1999, MNRAS, 308, 510
Martin, W. C., Musgrove, A., Saloman, E. B., et al. 2005, in NIST Atomic Spectra Database (Version 3.0), National Institute of Standards and Technology, Gaithersburg, MD, USA
Mathis, J. S. 1957, ApJ, 125, 318
Mokler, P. H., & Dunford, R. W. 2004, Phys. Scr., 69, C1
Möller, T., Beland, M., & Zimmerer, G. 1985, Phys. Rev. Lett., 55, 2145, 1985
Mollow, B. R. 1973, Phys. Rev. A, 8, 2684
Moses, D., Clette, F., Delaboudinière, J.-P., et al. 1997, Sol. Phys., 175, 571
Palmer, E. W., Hutley, M. C., Franks, A., et al. 1975, Rep. Prog. Phys., 38, 975
Peterson, J. R., & Bae, Y. K. 1986, Phys. Rev. A, 34, 3517
Ravindra, B., & Venkatakrishnan, P. 2003, Sol. Phys., 214, 267
Rayleigh, L. 1907, Phil. Mag., 14, 60
Redfield, S., Linsky, J. L., Ake, T. B., et al. 2002, ApJ, 581, 626
Rubin, M. H. 1996, Phys. Rev. A, 54, 5349
Schühle, U., Brown, C. M., Curdt, W., & Feldman, U. 1999, ESA-SP, 446, 617
Shapiro, J., & Breit, G. 1959, Phys. Rev., 113, 179
Spitzer, L., Jr., & Greenstein, J. L. 1951, ApJ, 114, 407
Tokaryk, D. W., Brooks, R. L., & Hunt, J. L. 1989, Phys. Rev. A, 40, 6113
Wilhelm, K., Curdt, W., Marsch, E., et al. 1995a, Sol. Phys., 162, 189
Wilhelm, K., Curdt, W., Marsch, E., et al. 1995b, in X-Ray and EUV/FUV Spectroscopy and Polarimetry, SPIE Proc., 2517, 2
Wilhelm, K., Lemaire, P., Curdt, W., et al. 1997, Sol. Phys., 170, 75
Wilhelm, K., Lemaire, P., Dammasch, I. E., et al. 1998, A&A, 334, 685
Wilhelm, K., Schühle, U., Curdt, W., et al. 2002, in The Radiometric Calibration of *SOHO*, ed. A. Pauluhn, M. C. E. Huber, R. V. Steiger (Noordwijk: ISSI/ESA), ISSI Scientific Report, SR-002, 145
Wood, R. W. 1902, Proc. Phys. Soc., 18, 396
Young, P. R., Dupree, A. K., Wood, B. E., et al. 2001, ApJ, 555, L121